Dalton Transactions

ROYAL SOCIETY OF CHEMISTRY

PAPER

View Article Online
View Journal | View Issue

Cite this: *Dalton Trans.*, 2021, **50**, 14038

$RbPb_8O_4Cl_9$: the first alkali metal lead oxyhalide with distorted $[PbO_3Cl_3]$ and $[PbOCl_5]$ mixed-anion groups†

Zhongxu Fan,‡[a] Chen Bai,‡[b,c] Hongsheng Shi,[b] Min Zhang,[b] Bei Zhang,[a] Jun Zhang *[a] and Junjie Li *[b]

Received 10th August 2021,
Accepted 1st September 2021

DOI: 10.1039/d1dt02665h

rsc.li/dalton

A new heavy metal oxychloride, $RbPb_8O_4Cl_9$, has been synthesized by a high-temperature solution method. The compound crystallizes in the centrosymmetric space group *P*4/*n* (no. 85) and exhibits a three-dimensional (3D) framework constructed from $[PbO_3Cl_3]$, $[PbOCl_5]$ and $[RbCl_8]$ polyhedra. $RbPb_8O_4Cl_9$ is an indirect band gap compound with an experimental band gap of 3.66 eV. The first-principles calculations indicate that the band gap mainly originated from the interaction of Pb 6p, O 2p and Cl 2p states. Meanwhile, the calculated birefringence of $RbPb_8O_4Cl_9$ is about 0.012 at 1064 nm. The compound is the first alkali metal lead oxyhalide, which enriches the structural diversity of oxyhalides and provides an insight for the exploration of new functional materials.

Introduction

The mixed-anion group, as a unique fundamental building block, provides an opportunity to produce advanced functional materials with abundant structural diversities and adjustable photoelectric properties.[1–4] Over the past few decades, a great number of mixed-anion compounds have been developed by a high- or low-temperature solution method in open/sealed systems, such as the compounds in AB_4O_6F (A = NH_4, Rb, Cs),[5–7] $AMoO_2F_3$ (A = K, Rb, Cs, NH_4, Tl),[8] Hg_3AsE_4X (E = S, Se; X = Cl, Br, I)[9] and $Pb_{13}O_6X_mY_{14-m}$ (X, Y = Cl, Br, I)[10] families. Nevertheless, the exploration of new mixed-anion materials with enhanced optical performances is still highly expected but challenging.[11–14]

Oxyhalides, with the combined structural and property advantages of oxides and halides, could be a promising system for the development of new photocatalysts, nonlinear optical crystals and infrared window materials, and have attracted great interest of many chemists and materials scientists recently.[15–19] Usually, for the optical materials applied in the infrared (IR) region, a wide IR transmission range is favorable.[20–23] To broaden the IR transmission region, the introduction of heavy metal atoms into oxyhalides has been demonstrated as a feasible way, since the vibrations of HM-O (HM = heavy metal atoms) bonding are usually located in the mid- or far-IR regions. For example, the peak for the vibration of the Pb–O bonding appears at 722 cm^{-1} (~14 μm).[9,24–26] Most recently, several research groups have made great progress in the development of lead-containing oxyhalide systems, and a series of new compounds, like $Pb_{17}O_8Cl_{18}$,[4] $Pb_3O_2Cl_2$,[16] $Ba_{27}Pb_8O_8Cl_{54}$,[27] $Ba_8SrPb_{24}O_{24}Cl_{18}$,[28] $Pb_{18}O_8Cl_{15}I_5$,[29] $Pb_{13}O_6Cl_4Br_{10}$,[10] $Pb_{13}O_6Cl_7Br_7$[10] and $Pb_{13}O_6Cl_9Br_5$[10] with wide IR transmission regions, have been discovered.

To further increase the structural and functional diversities of lead oxyhalides, the alkali metal lead oxyhalide system, M–Pb–O–Cl (M = alkali metal), was investigated in this work. The experimental parameters like the ratio of raw materials (RbCl, $PbCl_2$, PbO), reaction temperature and reaction time were studied systematically.[30–35] The first alkali metal lead oxyhalide $RbPb_8O_4Cl_9$ has been successfully synthesized by a high-temperature solution method in a sealed system. The compound crystallizes in the tetragonal (space group *P*4/*n*) lattice with a = 11.9557(3) Å, b = 11.9557(3) Å, c = 7.9620(4) Å, and Z = 2. $RbPb_8O_4Cl_9$ shows a 3D network structure built from unique $[PbO_3Cl_3]$ and $[PbOCl_5]$ mixed-anion and $[RbCl_8]$ single-anion groups. The optical and thermal properties of the title compound were investigated by Raman and UV-vis-NIR diffuse reflectance spectroscopy, differential scanning calorimetry

[a]*School of Physics Science and Technology, Xinjiang University, Urumqi 830046, Xinjiang, People's Republic of China. E-mail: zhj@xju.edu.cn*
[b]*CAS Key Laboratory of Functional Materials and Devices for Special Environments, Xinjiang Technical Institute of Physics & Chemistry, CAS, and Xinjiang Key Laboratory of Electronic Information Materials and Devices, 40-1 South Beijing Road, Urumqi 830011, China. E-mail: lijunjie@ms.xjb.ac.cn*
[c]*College of Chemistry and Chemical Engineering, Xinjiang Normal University, Urumqi, Xinjiang 830054, China*

†Electronic supplementary information (ESI) available. CCDC 2101780. For ESI and crystallographic data in CIF or other electronic format see DOI: 10.1039/d1dt02665h

‡These authors contributed equally to this work.

(DSC) technology and density functional theory (DFT) calculations. The experimental and theoretical results indicate that $RbPb_8O_4Cl_9$ is an indirect band gap compound with an experimental band gap of ~3.66 eV, and the theoretical birefringence of the compound is ~0.012 at 1064 nm.

Experimental section

Reagents and synthesis

The raw materials (RbCl, PbO, $PbCl_2$) with a purity of 99.99% (4N) were purchased from Aladdin Industrial Corporation. All the raw reagents were stored in a dry Ar-filled glove box with controlled oxygen and moisture levels below 0.1 ppm and used without further purification.

The single crystals of $RbPb_8O_4Cl_9$ for single-crystal X-ray diffraction measurement were synthesized by a high temperature solution method. Firstly, the mixture of RbCl, PbO and $PbCl_2$ with a molar ratio of 1 : 1 : 2 was weighed, ground and packaged in graphite crucibles under a dry atmosphere. Secondly, the crucibles were transferred into quartz tubes, and the quartz tubes were sealed with a methane–oxygen flame under a pressure of 10^{-3} Pa. After that, the samples were heated to 600 °C for 26 h and held for 24 h, and then cooled to room temperature in 8 days in a programmable muffle furnace. Finally, the air-stable transparent $RbPb_8O_4Cl_9$ single crystals were obtained successfully.

The pure phase $RbPb_8O_4Cl_9$ powder samples were synthesized by a high-temperature solid-state reaction. The mixture of RbCl, PbO and $PbCl_2$ with an atomic ratio of 1 : 4 : 4 was weighed and reacted in a sealed quartz tube. The experimental temperature program for the synthesis is as follows: the sealed quartz tubes with the starting materials were heated to 500 °C for 24 h from room temperature (25 °C) and kept at this temperature for 24 h. After that, the samples were cooled down to 350 °C for 150 h, followed by natural cooling to room temperature.

Single crystal X-ray diffraction

A high-quality transparent single crystal was used for the data collection. The crystal structure of $RbPb_8O_4Cl_9$ was determined at room temperature on a Bruker D8 Venture single-crystal X-ray diffractometer using the Mo-Kα radiation (λ = 0.71073 Å). Numerical absorption corrections were carried out using the SCALE program for the area detector and integrated with the SAINT program.[36,37] Then, the crystal structure was solved by direct methods and refined using the SHELXTL crystallographic software package. All atoms were refined with anisotropic displacement parameters. The program PLATON was used for verifying the possible missing symmetry elements, but no higher symmetries were found.[38] Finally, the crystal structure of $RbPb_8O_4Cl_9$ was confirmed. Table 1 presents the crystal data and structure refinements of the compound. The atomic coordinates, bond valence sum (BVS) calculations, bond distances and angles, and isotropic displacement parameters are presented in Tables S1–3 in the ESI.†

Table 1 Crystal data and structure refinements of $RbPb_8O_4Cl_9$

Empirical formula	$RbPb_8O_4Cl_9$
Formula weight	2126.04 g mol^{-1}
Temperature	293 K
Crystal system	Tetragonal
Space group	$P4/n$ (no. 85)
Unit cell dimensions	$a = b$ = 11.9557(3) (Å) c = 7.9620(4) (Å)
Volume	1138.08(8) Å^3
Z	2
Calculated density	6.204 g cm^{-3}
Absorption coefficient	62.128 mm^{-1}
Goodness-of-fit on F^2	1.099
Final R indices $[F_o^2 > 2\sigma(F_o^2)]^a$	R_1 = 0.0325, wR_2 = 0.0755
R indices	R_1 = 0.0381, wR_2 = 0.0823
Largest diff. peak and hole	1.696 e A^{-3} and −1.461 e A^{-3}

^{a} $R_1 = \sum||F_o| - |F_c||/\sum|F_o|$ and $wR_2 = [\sum w(F_o^2 - F_c^2)^2/\sum wF_o^4]^{1/2}$ for $F_o^2 > 2\sigma(F_o^2)$.

Powder X-ray diffraction

The purity of the synthesized $RbPb_8O_4Cl_9$ polycrystalline samples was verified by powder X-ray diffraction (PXRD), using a Bruker D2 Phaser diffractometer equipped with a diffracted beam monochromator set for Cu-Kα radiation (λ = 1.5418 Å). The PXRD pattern was recorded from 5° to 70° (2θ) with a scan step width of 0.01° and a fixed counting time of 1 s per step.

Energy dispersive X-ray spectroscopy (EDS)

The EDS spectrum of the $RbPb_8O_4Cl_9$ crystal was obtained using a field emission scanning electron microscope (FE-SEM, JEOL JSM-7610F Plus, Japan) with an energy dispersive X-ray spectrometer (Oxford, X-Max 50), which was operated at 5 kV.

Raman spectrum

The Raman spectrum was recorded for a $RbPb_8O_4Cl_9$ single crystal on a LabRAM HR Evolution spectrometer equipped with a CCD detector using 532 nm radiation from a diode laser. The $RbPb_8O_4Cl_9$ crystal was placed on a glass slide, and then an objective lens was used to choose a measured area on the crystal. A maximum power of 60 mW and a 35 μm (diameter) beam were used and the measurement was finished in 15 s.

UV-vis-NIR diffuse reflectance spectrum

The diffuse reflectance spectrum of pure phase $RbPb_8O_4Cl_9$ powder samples was recorded at room temperature using a Shimadzu SolidSpec-3700DUV spectrophotometer. The absorption spectrum was obtained from the reflection spectrum using the Kubelka–Munk formula: $\alpha/S = (1 - R)^2/(2R)$, in which α means the absorption coefficient, S is the scattering coefficient, and R is the reflectance.[39,40]

Thermal behaviour

The differential scanning calorimetry (DSC) curve of the title compound was obtained using a Netzsch STA 449 F3 simultaneous thermal analyzer. The sample was placed in a Pt crucible and heated at a rate of 5 °C min^{-1} in the range of 25–700 °C under a nitrogen gas flow.

Theoretical calculations

First-principles calculations based on density functional theory (DFT) for $RbPb_8O_4Cl_9$ were carried out using the CASTEP software package. The used exchange–correlation functional was the Perdew–Burke–Ernzerhof (PBE) functional within the generalized gradient approximation (GGA).[41–43] The kinetic energy cutoff was set as 820 eV. The *k*-points of the Monkhorst–Pack grids in the Brillouin zone were set as 4 × 4 × 2.[44] Because GGA usually underestimates the band gap due to the discontinuity of the exchange–correlation energy, scissors operators were used in the calculation of the band gap.[45] The linear optical properties (*e.g.*, refractive index) were obtained based on the Kramers–Kronig relation.

Results and discussion

Crystal structure

As shown in Table 1, $RbPb_8O_4Cl_9$ crystallizes in the tetragonal *P*4/*n* (no. 85) space group with *a* = 11.9557(3) Å, *b* = 11.9557(3) Å, *c* = 7.9620(4) Å, and *Z* = 2. In the structural determination of the title compound, the Rb atom was found to be disordered. In the asymmetric unit of $RbPb_8O_4Cl_9$, there is one crystallographically independent Rb atom, two Pb atoms, one O atom, and three Cl atoms. In $RbPb_8O_4Cl_9$, the Pb1 atoms are coordinated with three Cl atoms and three O atoms to make up the distorted $[PbO_3Cl_3]$ polyhedra (Fig. 1a) with the Pb–O bond length ranging from 2.274(7) to 2.373(8) Å and the Pb–Cl bond length ranging from 2.740(3) to 3.3046(5) Å. The Pb2 atoms are bonded to five Cl atoms and one O atom to construct the distorted $[PbOCl_5]$ polyhedra (Fig. 1b) with the Pb–O bond length ranging from 2.234(8) to 2.373(8) Å and the Pb–Cl bond length ranging from 2.740(3) to 3.3046(5) Å. The Rb atoms are bonded to eight Cl atoms to make up the $[RbCl_8]$ polyhedra (Fig. 1c) with the Rb–Cl bond length ranging from 3.370(5) to 3.410(5) Å and the Cl–Rb–Cl bond angle ranging from 66.40 (11)° to 169.99(18)°. The formed $[PbO_3Cl_3]$ and $[PbOCl_5]$ polyhedra are connected with each other to construct a porous network framework. To maintain the charge balance, the Rb atoms are located in the pores to build the final 3D network structure of $RbPb_8O_4Cl_9$, as shown in Fig. 1g. It is worth noting that the distorted $[PbO_3Cl_3]$ and $[PbOCl_5]$ groups in $RbPb_8O_4Cl_9$ are scarce in the reported lead oxyhalide, which are different from the formed $[PbO_2Cl_4]$, $[PbO_2Cl_2]$, and $[PbO_2Cl_3]$ mixed-anion groups in $Pb_3O_2Cl_2$ and $Pb_{17}O_8Cl_{18}$ (Fig. S1†).[4,16] Moreover, the crystal structure of $RbPb_8O_4Cl_9$ can also be described using the anion-central $[OPb_4]$ tetrahedra. As shown in Fig. 1d–g, four $[OPb_4]$ tetrahedra are connected with each other by edge-sharing to build a $[O_4Pb_8]$ tetramer. The $[O_4Pb_8]$ tetramers are linked by sharing the Cl3 atoms to form a $[Pb_8O_4Cl]$ chain-like structure (Fig. 1f). Furthermore, the $[Pb_8O_4Cl]$ chains are connected with each

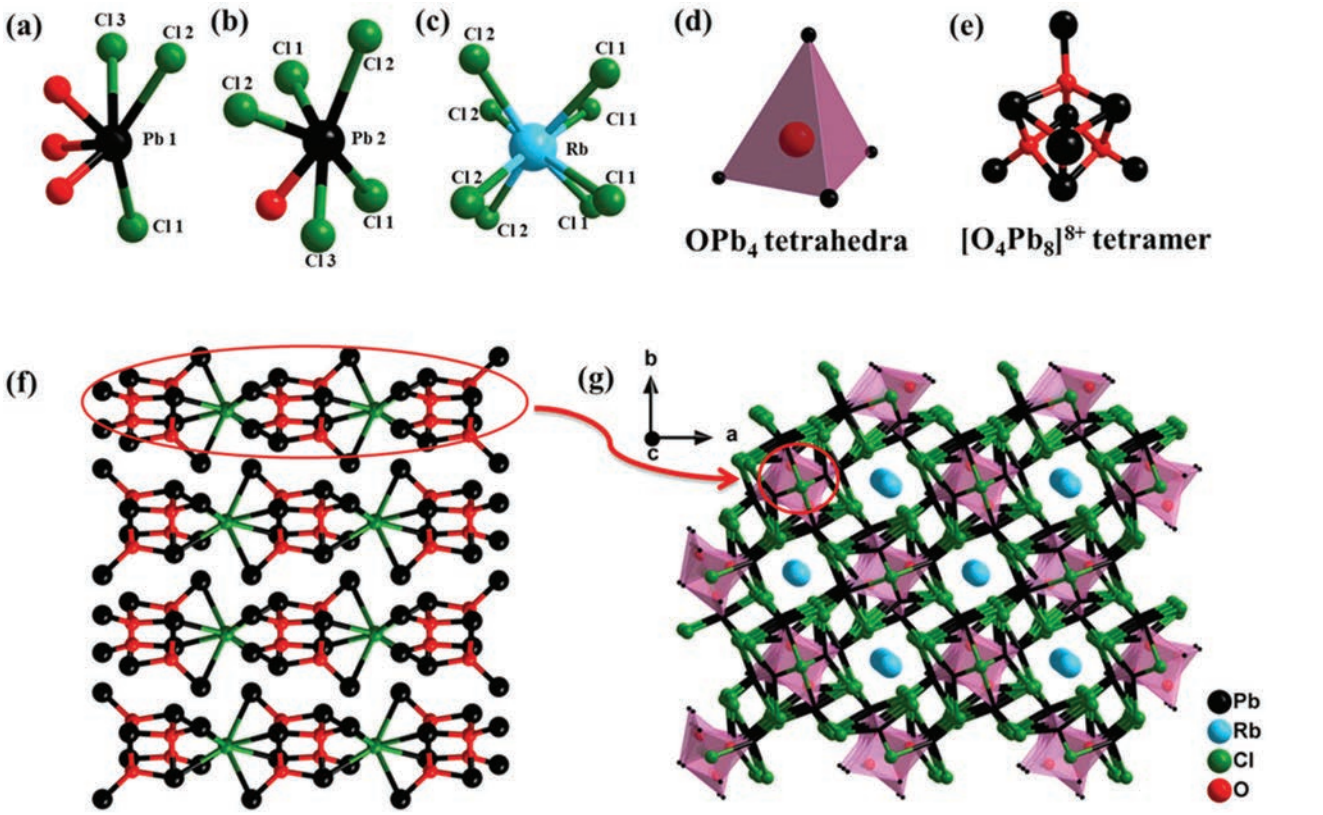

Fig. 1 (a–c) Coordination mode of Pb1, Pb2 and Rb; (d) OPb_4 tetrahedra; (e) $[O_4Pb_8]^{8+}$ tetramer; (f) $[Pb_8O_4Cl]$ chains; (g) the 3D structure of $RbPb_8O_4Cl_9$ viewed along the [001] direction.

other by sharing the Cl1 and Cl2 atoms to produce a porous 3D framework, and the Rb atoms are located in the pores to construct the final 3D network structure of the compound (Fig. 1g). The calculated bond valence sum (BVS) values of Pb (1), Pb(2), Rb(1), Rb(2), Cl(1), Cl(2), Cl(3) and O(1) are 2.12, 2.20, 1.09, 1.29, 1.03, 0.91, 0.95 and 2.42, respectively, which are in accordance with their corresponding oxidation states of +2, +1, −1, and −2 (Table S1†).

To confirm the results of single crystal XRD and to evaluate the optical properties, the pure phase $RbPb_8O_4Cl_9$ powder samples were synthesized by a high-temperature solid state reaction at about 500 °C. The XRD patterns of the synthesized $RbPb_8O_4Cl_9$ powder samples match well with the theoretical results derived from the $RbPb_8O_4Cl_9$ cif file (Fig. 2a), which confirms the results of single-crystal XRD and demonstrates the high purity of the synthesized powder samples. To further confirm the chemical composition and crystal structure of $RbPb_8O_4Cl_9$, the EDS and Raman spectra were obtained using the $RbPb_8O_4Cl_9$ single crystal samples. The EDS spectrum (Fig. 2b) demonstrates the existence of Rb, Pb, O and Cl elements in the crystal. In the Raman spectrum (Fig. 2c), the peaks at 70 and 96 cm^{-1} can be assigned to the stretching vibrations of the Rb–Cl bonding.[46] The peak at 138 cm^{-1} can be attributed to the stretching vibrations of the Pb–O bonding,[47] and the peak at 176 cm^{-1} should be related to the vibrations of the Pb–Cl bond in $RbPb_8O_4Cl_9$.[48]

To determine the experimental band gap of the title compound, the UV-vis-NIR diffuse reflectance spectrum was obtained. The results indicate that the optical band gap of $RbPb_8O_4Cl_9$ is 3.66 eV, which is larger than those of simple lead oxyhalides like $Pb_{17}O_8Cl_{18}$ (3.44 eV),[4] $Pb_{18}O_8Cl_{15}I_5$ (2.82 eV),[29] $Pb_{13}O_6Cl_4Br_{10}$ (3.05 eV),[10] $Pb_{13}O_6Cl_7Br_7$ (3.13 eV)[10] and $Pb_{13}O_6Cl_9Br_5$ (3.23 eV).[10] Detailed comparison of the band gaps is provided in Table S4.†

To clarify the thermal behavior of $RbPb_8O_4Cl_9$, the DSC experiment was conducted. The DSC curve in Fig. 3 shows that

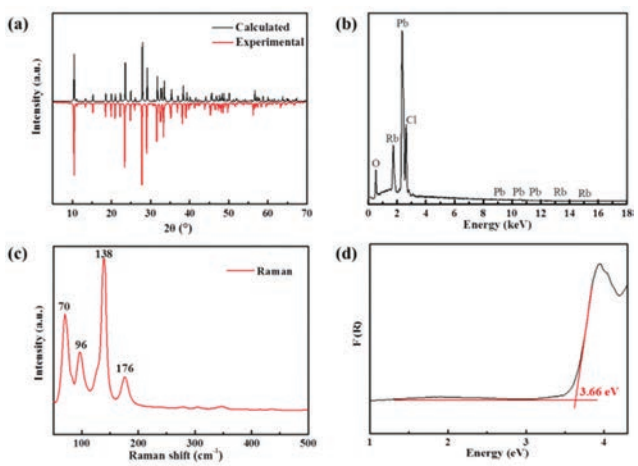

Fig. 2 Calculated (black) and experimental (red) XRD patterns (a); EDS spectrum (b); Raman spectrum (c); UV-vis-NIR diffuse reflectance spectrum (d) of $RbPb_8O_4Cl_9$.

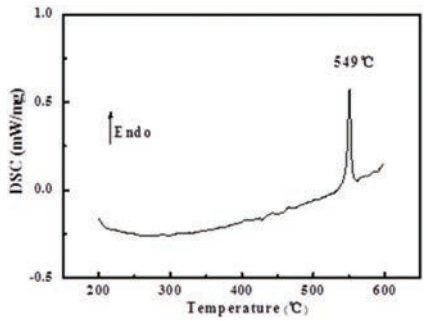

Fig. 3 DSC curve of $RbPb_8O_4Cl_9$.

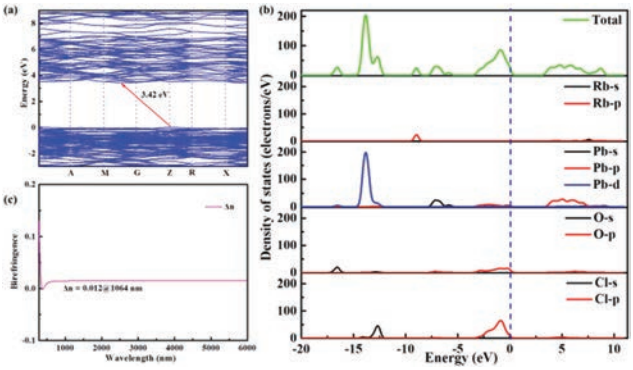

Fig. 4 (a) Calculated band structure; (b) total and partial density of states; (c) calculated birefringence of $RbPb_8O_4Cl_9$.

there is an evident endothermic peak at 550 °C during the heating process. To clarify the origin of the endothermic peak, the synthesized pure phase $RbPb_8O_4Cl_9$ powder samples were heated to 550 °C for 28 h in a muffle furnace. The discrepancy in the PXRD patterns before and after heating in Fig. S2† indicates that the endothermic peak should be related to the decomposition of $RbPb_8O_4Cl_9$, and the thermal decomposition products might be $Pb_3O_2Cl_2$, RbCl (↑) and $PbCl_2$ (↑). It means that $RbPb_8O_4Cl_9$ melts incongruently at 550 °C, and the flux method should be a good choice for the crystal growth.

To detect the origin of the optical properties in $RbPb_8O_4Cl_9$, DFT calculations were carried out. The calculated band structure (Fig. 4a) indicates that $RbPb_8O_4Cl_9$ is an indirect band gap compound with a band gap of 3.417 eV (Fig. 4a), which is consistent with the experimental result (3.66 eV). The total and partial densities of states imply that the band gap of $RbPb_8O_4Cl_9$ is mainly determined from the Pb 6p, O 2p and Cl 2p states. What's more, the calculated birefringence of $RbPb_8O_4Cl_9$ is about 0.012 at 1064 nm (Fig. 4c).

Conclusions

In summary, the M–Pb–O–Cl (M = alkali metal) alkali metal lead oxychloride system was investigated systematically, and the first alkali metal lead oxyhalide $RbPb_8O_4Cl_9$ was syn-

thesized successfully. The basic 3D framework structure of $RbPb_8O_4Cl_9$ was built from distorted $[PbO_3Cl_3]$ and $[PbOCl_5]$ polyhedra. The compound shows a large experimental band gap of 3.66 eV. The DFT calculations indicated that $RbPb_8O_4Cl_9$ is an indirect band gap compound, and the band gap is mainly determined from the Pb 6p, O 2p and Cl 2p states in the $[PbOCl_5]$ polyhedra. The results demonstrate the existence of the alkali metal lead oxyhalide, and shed light on the exploration of new functional materials in the alkali metal lead oxyhalide system.

Conflicts of interest

There are no conflicts to declare.

Acknowledgements

This work was supported by the High-level Talent Project of Xinjiang Uygur Autonomous Region (2020000039), S&T Partnership and International S&T Cooperation Program of Shanghai Cooperation Organization (2020E01040), the Tianshan Cedar Program (2019XS24), the National Natural Science Foundation of China (52002398, 22122509), the Youth Innovation Promotion Association of CAS (2020429), Quickly Supported Project (61409220136), and the West Light Foundation of the Chinese Academy of Sciences (Grant No. 2019-YDYLTD-002).

Notes and references

1 M. Xia, F. M. Li, M. Mutailipu, S. J. Han, Z. H. Yang and S. L. Pan, *Angew. Chem.*, 2021, **60**, 14650–14656.
2 W. Y. Zhang, W. Q. Jin, Z. H. Yang and S. L. Pan, *Dalton Trans.*, 2020, **49**, 17658–17664.
3 J. Z. Zhou, Y. Chu, J. J. Li and S. L. Pan, *Chem. Commun.*, 2021, **57**, 6440–6443.
4 H. Zhang, M. Zhang, S. L. Pan, X. Y. Dong, Z. H. Yang, X. L. Hou, Z. Wang, K. B. Chang and K. R. Poeppelmeier, *J. Am. Chem. Soc.*, 2015, **137**, 8360–8363.
5 G. Q. Shi, Y. Wang, F. F. Zhang, B. B. Zhang, Z. H. Yang, X. L. Hou, S. L. Pan and K. R. Poeppelmeier, *J. Am. Chem. Soc.*, 2017, **139**, 10645–10648.
6 Y. Wang, B. B. Zhang, Z. H. Yang and S. L. Pan, *Angew. Chem., Int. Ed.*, 2018, **57**, 2150–2154.
7 X. F. Wang, Y. Wang, B. B. Zhang, F. F. Zhang, Z. H. Yang and S. L. Pan, *Angew. Chem., Int. Ed.*, 2017, **56**, 14119–14123.
8 J. C. Hancock, M. L. Nisbet, W. G. Zhang, P. S. Halasyamani and K. R. Poeppelmeier, *J. Am. Chem. Soc.*, 2020, **142**, 6375–6380.
9 J. Beck, S. Hedderich and K. Kollisch, *Inorg. Chem.*, 2000, **39**, 5847–5850.
10 X. L. Chen, H. Jo and K. M. Ok, *Angew. Chem.*, 2020, **59**, 7514–7520.
11 M. Mutailipu, M. Zhang, B. B. Zhang, L. Y. Wang, Z. H. Yang, X. Zhou and S. L. Pan, *Angew. Chem., Int. Ed.*, 2018, **57**, 6095–6099.
12 B. B. Zhang, G. Q. Shi, Z. H. Yang, F. F. Zhang and S. L. Pan, *Angew. Chem., Int. Ed.*, 2017, **56**, 3916–3919.
13 Z. H. Yang, B. H. Lei, W. Y. Zhang and S. L. Pan, *Chem. Mater.*, 2019, **31**, 2807–2813.
14 G. M. Li, Z. H. Yang, J. J. Li and S. L. Pan, *Chem. Commun.*, 2020, **56**, 11565–11576.
15 A. Abudurusuli, J. B. Huang, P. Wang, Z. H. Yang, S. L. Pan and J. J. Li, *Angew. Chem.*, 2021, **60**, 2–8.
16 M. B. Sigman and B. A. Korgel, *J. Am. Chem. Soc.*, 2005, **127**, 10089–10095.
17 A. Abudurusuli, J. J. Li, T. H. Tong, Z. H. Yang and S. L. Pan, *Inorg. Chem.*, 2020, **59**, 5674–5682.
18 M. Lü, A. Aliev, J. Olchowka, M. Colmont, M. Huvé, C. Wickleder and O. Mentré, *Inorg. Chem.*, 2014, **53**, 528–536.
19 K. Feng, L. Kang, Z. S. Lin, J. Y. Yao and Y. C. Wu, *J. Mater. Chem. C*, 2014, **2**, 4590–4596.
20 X. M. Jiang, M. J. Zhang, H. Y. Zeng, G. C. Guo and J. S. Huang, *J. Am. Chem. Soc.*, 2011, **133**, 3410–3418.
21 C. Yang, X. Liu, C. Teng, X. Cheng, F. Liang and Q. Wu, *Mater. Today Phys.*, 2021, **19**, 100432.
22 B. W. Liu, H. Y. Zeng, X. M. Jiang and G. C. Guo, *CCS Chem.*, 2021, **3**, 964–973.
23 H. B. Gao, R. J. Chen, K. W. Zhang, A. Abudurusuli, K. R. Lai and J. J. Li, *Dalton Trans.*, 2021, **50**, 6315–6320.
24 I. T. Sorokina and K. L. Vodopyanov, *Solid-State Mid-Infrared Laser Sources*, Springer, Berlin, 2003.
25 L. Kang, D. M. Ramo, Z. S. Lin, P. D. Bristowe, J. G. Qin and C. T. Chen, *J. Mater. Chem. C*, 2013, **1**, 7363–7370.
26 M. Luo, F. Liang, Y. X. Song, D. Zhao, N. Ye and Z. S. Lin, *J. Am. Chem. Soc.*, 2018, **140**, 6814–6817.
27 X. X. Jiang, Z. Li, W. H. Xing, Z. S. Lin, J. Y. Yao and Y. C. Wu, *New J. Chem.*, 2020, **44**, 1699–1702.
28 Z. Li, S. Z. Zhang, W. H. Xing, Z. S. Lin, J. Y. Yao and Y. C. Wu, *Dalton Trans.*, 2020, **49**, 3667–3671.
29 X. L. Chen, Q. Jing and K. M. Ok, *Angew. Chem.*, 2020, **59**, 20323–20327.
30 Z. Li, S. Z. Zhang, W. L. Yin, Z. S. Lin, J. Y. Yao and Y. C. Wu, *Dalton Trans.*, 2018, **47**, 17198–17201.
31 M. Abudoureheman, S. J. Han, Y. Wang, B. H. Lei, Z. H. Yang and S. L. Pan, *Inorg. Chem.*, 2017, **56**, 3939–3945.
32 Y. N. Chen, M. Zhang, C. Hu, Z. H. Yang and S. L. Pan, *Inorg. Chem. Front.*, 2018, **5**, 1787–1794.
33 M. Wen, C. Hu, Z. H. Yang, X. H. Wu and S. L. Pan, *Dalton Trans.*, 2018, **47**, 9453–9458.
34 Y. Yang, B. B. Zhang, X. W. Wu and K. Wu, *Dalton Trans.*, 2021, **50**, 4129–4132.
35 L. H. Gao, G. Bian, Y. Yang, B. B. Zhang, X. Y. Wu and K. Wu, *New J. Chem.*, 2021, **45**, 12362–12366.
36 *SAINT, version 7.60A, Bruker Analytical X-ray Instruments, Incorporated*, Madison, WI, 2008.
37 Y. Chu, P. Wang, H. Zeng, S. C. Cheng, X. Su, Z. H. yang, J. J. Li and S. L. Pan, *Chem. Mater.*, 2021, **33**, 6514–6521.

38 A. L. Spek, *J. Appl. Crystallogr.*, 2003, **36**, 7–13.
39 J. Tauc, *Mater. Res. Bull.*, 1970, **5**, 721–729.
40 P. Kubelka and F. Munk, *Tech. Phys.*, 1931, **12**, 593–601.
41 S. J. Clark, M. D. Segall, C. J. Pickard, P. J. Hasnip, M. J. Probert, K. Refson and M. C. Payne, *Z. Kristallogr.*, 2005, **220**, 567–570.
42 D. M. Ceperley and B. J. Alder, *Phys. Rev. Lett.*, 1980, **45**, 566–569.
43 H. J. Monkhorst and J. D. Pack, *Phys. Rev. B: Solid State*, 1976, **13**, 5188–5192.
44 J. P. Perdew and A. Zunger, *Phys. Rev. B: Condens. Matter Mater. Phys.*, 1981, **23**, 5048–5079.
45 J. P. Perdew and Y. Wang, *Phys. Rev. B: Condens. Matter Mater. Phys.*, 1992, **45**, 13244–13249.
46 I. R. Nair and C. T. Walker, *Phys. Rev. B: Solid State*, 1973, **7**, 2740–2754.
47 H. Z. Jia, G. H. Chen and W. C. Wang, *Opt. Mater.*, 2006, **29**, 445–448.
48 H. D. Lutz, K. Beckenkamp and S. Peter, *Spectrochim. Acta*, 1994, **51**, 755–767.